Int. J. Heat Mass Transfer. Vol. 31, No. 4, pp. 731–742, 1988
Printed in Great Britain

0017–9310/88 $3.00 + 0.00

Local evaporative heat transfer coefficient in turbulent free-falling liquid films

J. A. SHMERLER† and I. MUDAWWAR
Boiling and Two-phase Flow Laboratory, School of Mechanical Engineering,
Purdue University, West Lafayette, IN 47907, U.S.A.

(*Received* 4 *June* 1987 *and in final form* 19 *August* 1987)

Abstract—Evaporative heating of a free-falling turbulent liquid film has been investigated experimentally and numerically. The film exhibited a long thermal development length persisting up to more than one half of the 781 mm long heated test section. The increased length of the development region is attributed to the formation of a boundary layer at the film interface. This boundary layer was predicted numerically and observed in temperature measurements within the film. The heat transfer coefficients are averaged over the lower section of the tube and correlated as a function of the Reynolds and Prandtl numbers. Numerical predictions are made for the development region and for fully developed heat transfer coefficients using three different eddy diffusivity models. Comparison with experimental data reveals that two of these models are fairly successful in predicting the extent of the thermal development region and the time-averaged evaporative heat transfer coefficient; yet the data indicate the need for development of a new model which accurately accounts for local and spatial wave-induced variations of film thickness.

1. INTRODUCTION

THE CHARACTERISTICS of free-falling evaporating films are of importance in many aspects of thermal engineering and chemical processes. While a need has been shown for an improved understanding of falling film transport processes, the amount of heat transfer data remains limited as shown by the summary of experimental investigations in Table 1.

The study by Chun and Seban [2] is the most often sighted reference on evaporative heating of falling films. They presented correlations for heat transfer coefficients in the wavy laminar and the turbulent regimes as functions of the Reynolds and Prandtl numbers. They also found a correlation for the transition Reynolds number as a function of Prandtl number. Fujita and Ueda [3] presented evaporation data at a pressure of 1 atm. Their data followed the trends shown by Chun and Seban but were an average of 10% higher.

While the experimental work is limited, many eddy diffusivity models have been developed specifically for predicting heat transfer coefficients for falling films [4–15]. The majority of these models use a modified Van Driest function near the wall and a damping function to model the turbulent activity at the film interface. Mills and Chung [8] presented a model that uses a modified Van Driest function and a heat–mass transfer analogy with the gas absorption results of Lamourelle and Sandall [16] to model the eddy diffusivity near the film interface. Hubbard *et al.* [11] used a similar approach with the addition of new gas absorption data and the effects of concurrent vapor flow. Seban and Faghri [12] looked at several modeling schemes in an attempt to predict Chun and Seban's data and new data collected on essentially the same apparatus as Chun's [17]. They concluded that the best predictions are made using Limberg's [9] model near the wall, modified with the interface damping function of Mills and Chung. Although their model predicts the data reasonably well, a physical inconsistency occurs as there is a discontinuity between the two functions. Mudawwar and El-Masri [15] presented an eddy diffusivity function which combines the Van Driest damping function and the experimental turbulence data of Ueda *et al.* [18] to produce an eddy diffusivity profile that is continuous over the entire film thickness.

All of the turbulence models are semi-empirical, but are based on a very limited data base. The present study provides a new data base by obtaining heat transfer coefficients over a wide range of Reynolds and Prandtl numbers. A test section 781 mm long was used to determine heat transfer coefficients during thermal development and in the fully developed regime, and to determine the behavior of the temperature profile across the film thickness. A numerical study was also performed to determine how well the available turbulence models predict the new data.

2. EXPERIMENTAL SYSTEM

The experimental apparatus was the same as that described in ref. [19]. The test section shown in Fig. 1 was 25.4 mm in diameter and consisted of a 300 mm long porous plastic film distributor, a 757 mm long

† Current address: AT&T Bell Laboratories, Liberty Corners, NJ 07060, U.S.A.

NOMENCLATURE

g	acceleration due to gravity
h_E	heat transfer coefficient for evaporative heating, $q_w/(T_w - T_{sat})$
h_E^*	dimensionless heat transfer coefficient, $(h_E v^{2/3})/(kg^{1/3})$
k	thermal conductivity
Ka	Kapitza number, $(\mu^4 g)/(\rho\sigma^3)$
L	length of the heated section
Pr	Prandtl number
Pr_t	turbulent Prandtl number, $\varepsilon_m/\varepsilon_h$
q	local heat flux
q_w	wall heat flux
Re	Reynolds number, $4\Gamma/\mu$
T	local temperature
T_{in}	inlet temperature
T_m	mean temperature
T_s	interface temperature
T_{sat}	saturation temperature
T_w	wall temperature
T^+	dimensionless temperature, $\rho c_p u^*(T_w - T)/q_w$
u	local velocity component in the flow direction
u^*	friction velocity, $\sqrt{(\tau_w/\rho)}$
u^+	dimensionless film velocity, u/u^*
x	longitudinal position from the entrance to the heated section
y	distance from the solid wall
y^+	dimensionless distance from the solid wall, yu^*/v.

Greek symbols

α	thermal diffusivity
Γ	mass flow rate per unit film width
δ	film thickness
δ^+	dimensionless film thickness, $\delta u^*/v$
ε_h	eddy heat diffusivity
ε_m	eddy momentum diffusivity
μ	dynamic viscosity
ν	kinematic viscosity
ρ	liquid density
σ	surface tension
τ	local shear stress
τ_w	wall shear stress.

Table 1. Experimental studies on evaporative heating of falling films

	Author			
	Struve [1]	Chun and Seban [2]	Fujita and Ueda [3]	Present study
Injection method	nozzle	sintered tube	sintered tube (152 mm)	porous plastic (300 mm)
Tube diameter	32 mm o.d. 26 mm i.d.	28.6 mm o.d. 28.4 mm i.d.	16 mm o.d. 14 mm i.d.	25.4 mm o.d. 24.6 mm i.d.
Adiabatic length	0	317.5 mm	250 mm copper rod	757 mm
Heated length	1250 mm	292 mm	600 and 1000 mm	781 mm
Heating method	steam condensation	electrical resistance	electrical resistance	electrical resistance
Test fluid	R11	water	water	water
Reynolds number	≈70–8800	320–21 000	700–9100	5000–37 500
Prandtl number	4.12	1.77–5.7	1.8–2.0	1.75–5.4

adiabatic hydrodynamic development section made of G-10 fiberglass based phenolic plastic, and heated length of 781 mm. The latter was a polished stainless steel tube with a wall thickness of 0.41 mm through which a high d.c. current was passed to produce a constant wall flux.

Heat transfer coefficients were determined from the difference between the wall temperature and the saturation temperature. Pairs of thermocouples 180° apart at 17 locations along the heated length measured the inside wall temperature. The pairs were unequally spaced with the thermocouples grouped closer together at the top of the heated length to monitor thermal boundary layer development. The outside wall temperature was calculated from these measurements by performing a control volume energy balance assuming an adiabatic inner surface and uniform volumetric heat generation within the stainless steel tube. Reference [19] describes the apparatus and thermocouple locations in detail. The saturation temperature was both measured and calculated from the chamber pressure, determined from measurements made with a high accuracy pressure transducer.

All tests were performed using deionized water which was deaerated before introduction into the experimental apparatus. A vacuum pump removed noncondensible gases from the system to give pure saturated conditions within the flow loop. After charging the system and achieving equilibrium pressure and temperature conditions, fluid was circulated at the maximum flow rate to give the greatest film thickness. The selected operating conditions were achieved through the control of the chamber pressure and inlet temperature of the fluid. The temperature

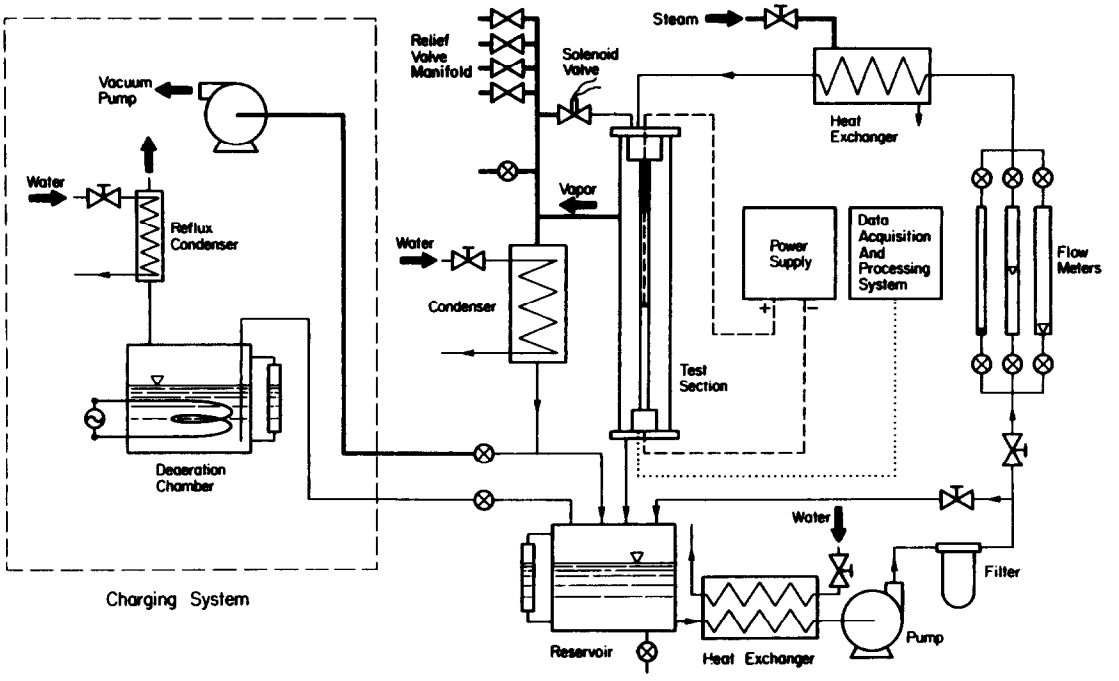

FIG. 1. Schematic diagram of the fluid delivery system.

was controlled through a heat exchanger located upstream of the test chamber. The pressure was maintained at a level equal to the saturation value by controlling the condensation rate of the generated vapor, which was achieved by adjusting the amount of coolant passing through the condensing heat exchanger. At high power levels, where a large amount of vapor was generated, a vacuum pump supplemented the condenser.

During the tests, the power level was kept below the wall heat flux necessary for the onset of nucleate boiling (ONB). This value was determined from a manipulation of a correlation for ONB presented in ref. [20] using the correlation for the evaporation heat transfer coefficient presented by Chun and Seban [2]. The wall heat flux was always kept at least 25% below the value determined to produce boiling incipience.

Temperature measurements along the heated length were recorded upon reaching steady-state conditions. New test conditions were achieved by decreasing the flow rate to give a new Reynolds number, adjusting the condensate rate to maintain the desired saturation level, and adjusting the power to the proper level. This procedure was continued until any further decrease in flow rate caused film dryout. The flow rate was then increased to the maximum value and the chamber pressure was modified to give different saturated conditions.

3. EXPERIMENTAL RESULTS

Heat transfer results for films undergoing evaporative heating have been obtained over a Reynolds number range of 4990 to 37 620 for Prandtl numbers

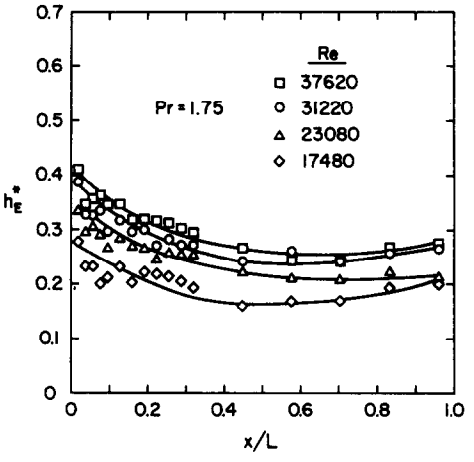

FIG. 2. Variation of the evaporative heat transfer coefficient with distance along the heated section for $Pr = 1.75$.

between 1.75 and 5.42. Figures 2–5 show typical results for the heat transfer coefficient as a function of position along the heated length. A complete documentation of the local heat transfer data and operating conditions of this study can be found in ref. [21]. The position is normalized with respect to the total heated length, L, and the fluid properties are based on the saturation temperature. The thermal development region persisted over more than one half of the heated length, longer than that observed during tests involving sensible heating of falling films [19]. This increased development length is attributed to boundary layer development at the film interface.

Figure 6 is a qualitative comparison of two films: one undergoing sensible heating, and the other, evap-

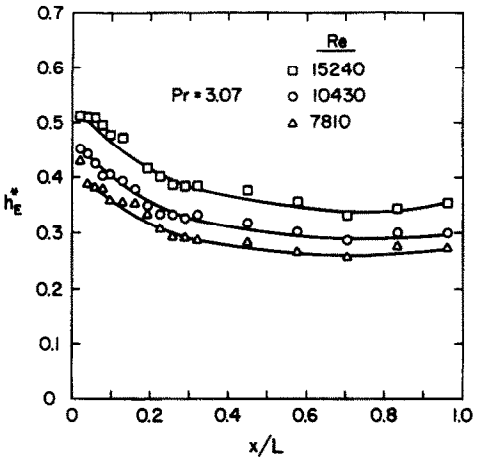

FIG. 3. Variation of the evaporative heat transfer coefficient with distance along the heated section for $Pr = 3.07$.

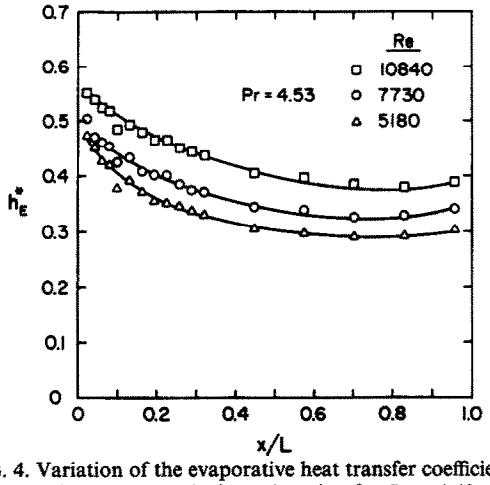

FIG. 4. Variation of the evaporative heat transfer coefficient with distance along the heated section for $Pr = 4.43$.

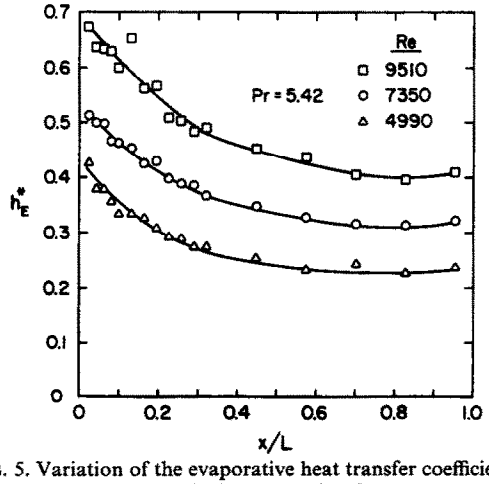

FIG. 5. Variation of the evaporative heat transfer coefficient with distance along the heated section for $Pr = 5.42$.

orative heating. For the former, the interface is defined as adiabatic. After the establishment of the wall boundary layer, the energy input at the wall increases the bulk temperature of the fluid, while maintaining a constant wall to surface temperature differential. At this point, fully developed conditions are achieved. A saturated film initially undergoes a development process like that for sensible heating with the generation of a thermal boundary layer at the wall. When the effects of the wall flux reach the film interface, evaporative mass transfer causes energy loss. The heat transfer at the film interface creates a temperature differential within the liquid which delays the formation of a fully-developed temperature profile and results in a longer development length.

The crude qualitative description of thermal boundary layer development in Fig. 6 does not take into account the temperature differential associated with interface mass transfer. During evaporation, the rate of departure of molecules from the liquid film into the vapor region exceeds the rate of arrival of molecules from the vapor towards the interface. The net molecular transfer gives rise to an interfacial thermal resistance; yet, for water at the pressures under consideration, this thermal resistance is negligible by comparison to the thermal resistance across the film [22].

Evidence of the liquid thermal resistance near the interface was observed during experiments in which a thermocouple embedded in the leading edge of a film sampling scoop was traversed across the film. Reference [19] describes the sampling scoop in detail. Temperatures recorded at discrete positions from the heated wall allowed for a qualitative assessment of the temperature profile. Figure 7 shows some typical results. The position has been nondimensionalized with respect to the film thickness determined from the empirical correlation presented by Gimbutis [10] ($\delta_G = 0.136(v^2/g)^{1/3}Re^{0.583}$). The temperature bands represent the high and low turbulent temperature fluctuations measured by the scoop thermocouple. Since the film is wavy, the measurement position $\delta = \delta_G$ does not necessarily correspond to the film interface. Rather, temperature fluctuations at $\delta = \delta_G$ are caused by eddy activity within the liquid as well as the intermittence of liquid and vapor phases. Figure 7 shows a sharp and thin wall boundary layer followed by the bulk of the film at a fairly constant temperature slightly greater than T_{sat}. As the interface of the film is approached a sharp temperature differential appears. This differential was not present for films undergoing sensible heating. Figure 7 contrasts the temperature profiles for an evaporating and sensibly heated film. The temperature has been nondimensionalized with respect to the measured value of the mean temperature to allow easier comparison of the two cases. Both show a similar profile near the wall, but differ at the film interface. For the sensibly heated film, the profile is representative of an adiabatic interface. For the evaporative case, a large gradient exists as a result of the energy loss at the interface, and as mentioned previously causes the increased development length.

Beyond the initial development region the decrease in the heat transfer coefficient in Figs. 2–5 slowed, but never showed true asymptotic behavior. In some

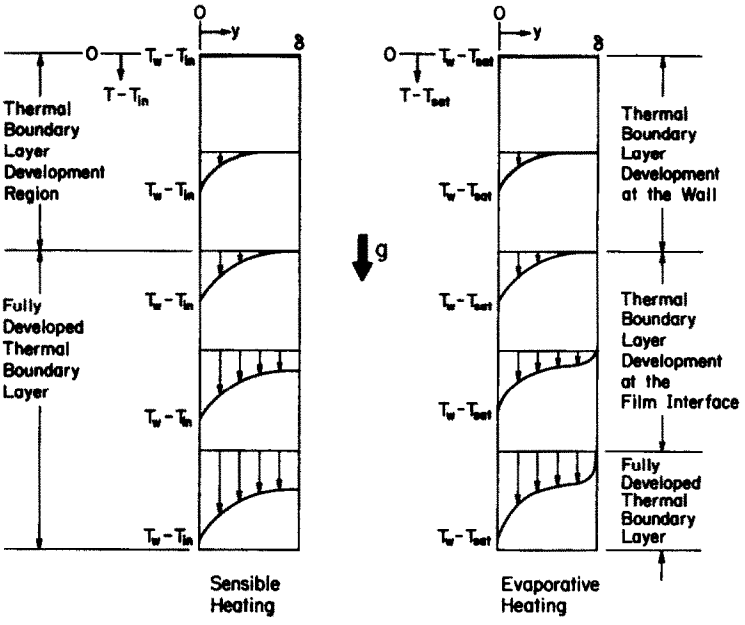

FIG. 6. Development of the thermal boundary layer for hydrodynamically fully developed film flow over a uniformly heated wall for the cases of sensible and evaporative heating.

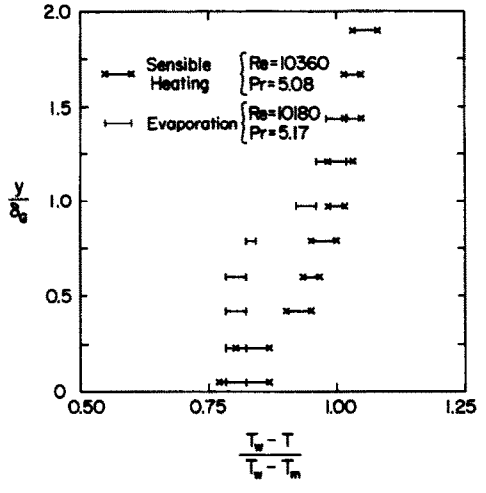

FIG. 7. Comparison of temperature profiles across the film for the cases of sensible and evaporative heating.

cases, the heat transfer coefficient showed a slight enhancement over the last two measurement positions (650 and 750 mm from the start of the heated length). This enhancement was a result of increased turbulent activity caused by longitudinal changes in interfacial waves.

To better understand the effects of interfacial waves on turbulent velocity fluctuations, videographic analysis of film motion was employed for representative operating conditions. Individual frame analysis revealed the existence of interfacial waves covering a wide spectrum of wavelengths. An independent study was also conducted to measure film thickness fluctuations on a vertical adiabatic column using water as the working fluid. A high resolution conductance probe recently developed by Koskie *et al.* [23] at Purdue's Boiling and Two-phase Flow Laboratory was employed in this study. A time record of interfacial waves was obtained at a position 1895 mm below the lower end of the porous injection section. Typical variation of local film thickness is shown in Fig. 8. Waves formed at the film interface appear to be a combination of large waves with small ripples superimposed on the large waves. Strong spectral components for large and small waves were typically in the range of 10–20 and 75–150 Hz, respectively. Film waviness is complicated further by variations in both the instantaneous and the time-averaged values of film thickness with film travel. According to a study by Takahama and Kato [24], the minimum film thickness decreases in the direction of fluid flow, while the maximum thickness increases fairly linearly with distance as more film mass is accumulated into larger and faster waves. The severe fluctuations of instantaneous film thickness from their time-averaged values and the longitudinal changes in wave characteristics are strong evidence against common belief that an idealized smooth interface is a reasonable representation of film flow.

The work by Brumfield and Theofanous [25] represents the only systematic attempt known to the authors of predicting the evaporative heat transfer coefficient across turbulent wavy films. They used film hydrodynamics data determined by Telles [26] and Chu and Dukler [27] to develop a coherent transport model which accounts for film thickness fluctuations. The model was used to predict heat transfer data for free-falling and shear-driven films using wave parameters correlated experimentally at $Pr \sim 5.7$. Since there is no firm basis for predicting wave parameters

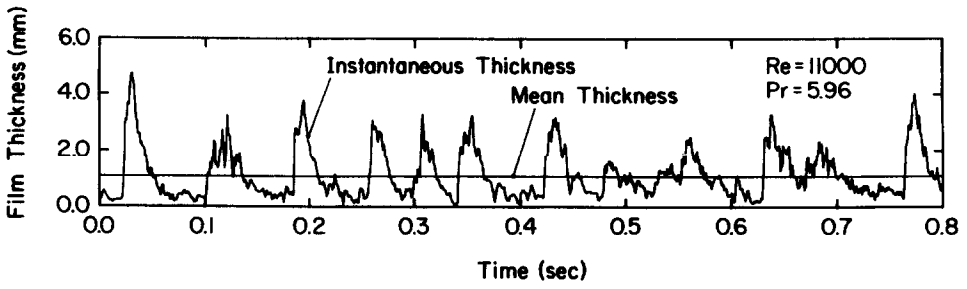

FIG. 8. Film thickness variation with time for an adiabatic water film at 26°C.

for different fluids or for temperatures corresponding to different Prandtl numbers, the usefulness of the Brumfield and Theofanous model is limited by the availability of film hydrodynamics data for the corresponding fluid and operating conditions. Furthermore, hydrodynamic correlations obtained from adiabatic film experiments may not apply for films subjected to evaporative heating due to the sensitivity of surface tension to temperature gradients along the film interface.

The developmental nature of the film precludes the determination of a universal correlation for a fully developed heat transfer coefficient. A correlation was determined for h_E^* averaged over the positions corresponding to $x/L = 0.576$, 0.704 and 0.832 from the inlet to the heated length. These positions were chosen because the heat transfer coefficient appeared to exhibit a minimum value for all the tests in this area. As shown in Fig. 9 the average heat transfer coefficient was correlated as a function of the Reynolds and Prandtl numbers as follows:

$$h_E^* = 0.0038 Re^{0.35} Pr^{0.95}. \quad (1)$$

The correlation has an average error of 6%, a maximum error of 14.9% and a standard deviation of 0.023 and all fluid properties are based on the saturation temperature.

The Prandtl number exponent in equation (1) exceeds that of Chun and Seban's correlation ($h_E^* = 0.0038 Re^{0.4} Pr^{0.65}$). Since this exponent is much greater than that associated with single-phase forced convection ($Nu \propto Pr^{0.33}$), heat transfer near the film interface must occur by a different transport mechanism. Due to limitations of the present data base, the dependence of the heat transfer coefficient on parameters other than the Reynolds and Prandtl numbers, such as the Kapitza number, Ka, could not be assessed. It is well known that surface tension forces both influence the interfacial wave characteristics and dampen turbulent velocity fluctuations near the film interface. Interfacial instabilities may also be amplified by surface tension gradients associated with temperature variations along the film interface. Since the Kapitza number is proportional to μ^4, the high Prandtl number exponent in equation (1) may indirectly account for these effects.

Figure 10 shows a comparison between the present data and the data presented by Chun for the heat transfer coefficient as a function of position along the heated length. Chun's data are nondimensionalized with respect to the length of the heated section used in the present study. For higher Prandtl numbers, the slopes are similar near the top of the heated length, but Chun's data begins to level off earlier. The short length of Chun's test section, 292 mm, prevented the determination of downstream effects. At lower Prandtl numbers, there is a much steeper gradient at the start of the heated length, after which similar slopes can be observed. Chun's data do not appear to reach a fully developed state since the test section length prevented any further measurements.

Figure 11 is a comparison of Chun and Seban's heat transfer correlation with the present correlation. The agreement at higher Prandtl numbers is good, but there is a large difference at the lower Prandtl number of 1.75. This difference could be a result of the occurrence of nucleate boiling or subcooled inlet conditions in Chun's experiments, or due to data in the thermal development region used in his correlation. In Chun's experiments, at a pressure of 1 atm, and at lower

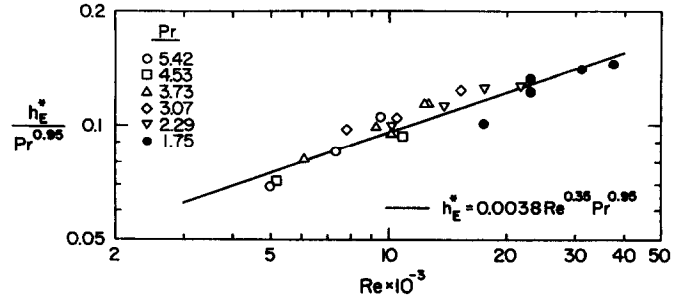

FIG. 9. Correlation of the evaporative heat transfer coefficient for Re = 4990–37 620 and Pr = 1.75–5.42.

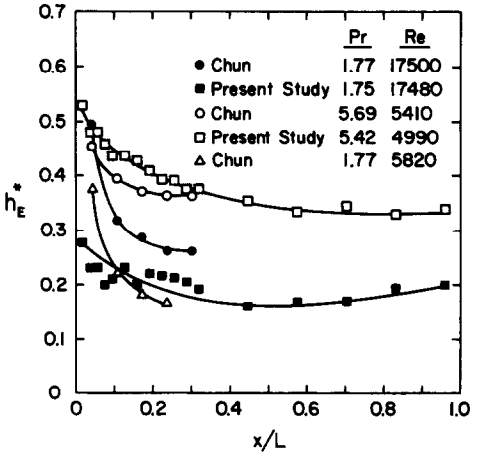

FIG. 10. Comparison of the variation of the evaporative heat transfer coefficient along the heated length obtained in the present study and in Chun's experiments [17].

Reynolds numbers, the value for the wall flux was sometimes greater than the theoretical value for the onset of nucleate boiling. Under these instances, the fully developed value for h_E^* was taken at the position before nucleation occurred, even if it was still in the development region. The presence of subcooled inlet conditions in Chun's experiments (up to 3.39°C) could also be responsible for the higher heat transfer coefficients as well as the steeper temperature gradients seen in Fig. 10. Chun's calculations to determine h_E^* assume that the film enters the heated length at T_{sat}. If a film enters subcooled, the temperature difference based on T_{sat} would be smaller than that actually seen by the film $(T_w - T_{in})$, resulting in a higher calculated value for h_E^*. In the present study, a sampling scoop was used to measure the film temperature near the start of the heated length to insure that the film was at the desired saturation temperature corresponding to the measured chamber pressure.

4. NUMERICAL RESULTS

As shown in Section 3, neglecting the effects of interfacial waves represents an oversimplification of transport phenomena in falling films. Yet, empirical or semi-empirical models are very desirable in many applications involving thin films, and a comparison of numerical results based on these models to experimental data can provide better guidance in the selection of suitable approximate film models.

Numerical predictions were made to determine heat transfer coefficients for the thermal development of a saturated film and for films that have reached fully developed conditions. The momentum and energy equations for a hydrodynamically developed free-falling film take the following form [15]:

$$\tau = \rho(\nu + \varepsilon_m)\frac{du}{dy} \tag{2}$$

$$u\frac{\partial T}{\partial x} = \frac{\partial}{\partial y}\left[\left(\alpha + \frac{\varepsilon_m}{Pr_t}\right)\frac{\partial T}{\partial y}\right] \tag{3}$$

with the following boundary conditions for a film undergoing evaporative heating:

$$x = 0 \quad T = T_{sat}$$

$$y = 0 \quad \frac{\partial T}{\partial y} = \frac{-q_w}{k}$$

$$y = \delta \quad T = T_{sat}.$$

The turbulence terms were modeled using the eddy diffusivity functions presented by Hubbard *et al.* [11], Limberg [9], and Mudawwar and El-Masri [15] which employ a modified Van Driest equation near the wall, but use different approaches to determine the eddy diffusivity at the film interface. Hubbard *et al.*'s model uses an analogy to mass transfer correlations obtained for gas absorption into a falling film; Limberg's model assumes a constant value for ε_m/ν over the outer 40% of the film thickness away from the wall, and Mudawwar and El-Masri's model uses experimental turbulence data to obtain a smooth eddy diffusivity profile over the film thickness. A Prandtl number of 0.9 was used with all of the models. Limberg's model is fundamentally different from the other models since it does not take into direct account the effect of surface damping on the interfacial thermal resistance.

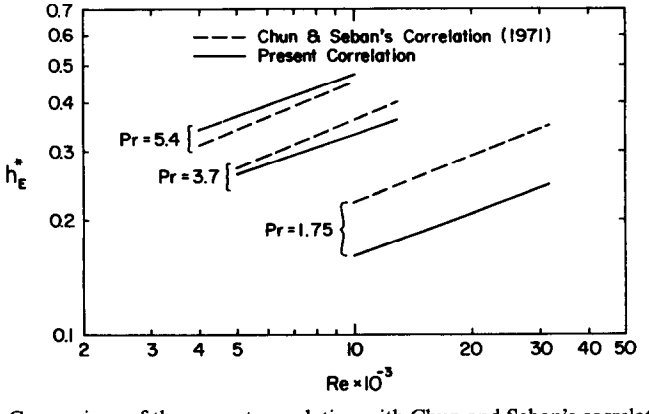

FIG. 11. Comparison of the present correlation with Chun and Seban's correlation [2].

Table 2. Turbulence models for free-falling films used for comparison with experimental data

Author	Range	Eddy diffusivity
Limberg [9]	$0 \leqslant y^+ < 0.6\delta^+$	$\frac{\varepsilon_m}{\nu} = -\frac{1}{2} + \frac{1}{2}\sqrt{\left\{1+4K^2y^{+2}\left[1-\exp\left\{\frac{-y^+\left(1-\frac{y^2}{\delta^+}\right)^{1/2}}{A^+}\right\}\right]^2\left(1-\frac{y^+}{\delta^+}\right)\exp\left(-3.32\frac{y^+}{\delta^+}\right)\right\}}$
	$0.6\delta^+ \leqslant y^+ \leqslant \delta^+$	$\frac{\varepsilon_m}{\nu} = \frac{\varepsilon_m}{\nu}\Big\vert_{y^+=0.6\delta^+}$
		$K = 0.41;\ A^+ = 25.1$
		$Pr_t = 0.89$
Hubbard *et al.* [11]	$0 \leqslant y^+ < y_i^+$	$\frac{\varepsilon_m}{\nu} = -\frac{1}{2} + \frac{1}{2}\sqrt{\left\{1+4K^2y^{+2}\left[1-\exp\left(1-\frac{y^+}{\delta^+}\right)\right]^2\left(1-\frac{y^+}{\delta^+}\right)\right\}}$
	$y_i^+ \leqslant y^+ \leqslant \delta^+$	$\frac{\varepsilon_m}{\nu} = \frac{8.13\times10^{-17}}{Ka}\cdot\frac{Re^{2m}}{\delta^{+2/3}}(\delta^+ - y^+)^2$
		$K = 0.4;\ A^+ = 25;\ m = 6.95\times10^2\nu^{1/2}$, ν in $m^2\,s^{-1}$
		$Pr_t = 0.9, 1.0, 1.1$
Mudawwar and El-Masri [15]	$0 \leqslant y^+ \leqslant \delta^+$	$\frac{\varepsilon_m}{\nu} = -\frac{1}{2} + \frac{1}{2}\sqrt{\left\{1+4K^2y^{+2}\left(1-\frac{y^+}{\delta^+}\right)^2 \times\left[1-\exp\left\{-\frac{y^+}{26}\left(1-\frac{y^+}{\delta^+}\right)^{1/2}\left(1-\frac{0.865Re_{crit}^{1/2}}{\delta^+}\right)\right\}\right]^2\right\}}$
		$Re_{crit} = \frac{0.04}{Ka^{0.37}}$
		$K = 0.40;\ A^+ = 26$
		$Pr_t = 1.4\exp\left(-15\frac{y^+}{\delta^+}\right) + 0.66$

Numerical predictions of the Limberg model are compared to those of the other two models to demonstrate the significance of interfacial damping on the development of the thermal boundary layer in evaporating films.

In the first part of this study, fully developed heat transfer coefficients ($\partial T/\partial x = 0$) were predicted as a function of Reynolds number. The Reynolds number was derived from the momentum equation by first determining the velocity distribution, and then integrating the velocity over the film thickness. The film is assumed to have a constant thickness by neglecting wave effects, and the mass lost by evaporation is assumed to be a small fraction of the total mass flow rate of the film. In dimensionless terms, the equations for the velocity distribution and Reynolds number are as follows [15]:

$$u^+ = \int_0^{y^+} \frac{1 - y^+/\delta^+}{1 + \varepsilon_m/\nu}\,dy^+ \tag{4}$$

$$Re = 4\int_0^{\delta^+} u^+\,dy^+. \tag{5}$$

The heat flux can be nondimensionalized with respect to the wall heat flux. That is

$$\frac{q}{q_w} = \frac{1}{Pr}\left[1 + \frac{Pr}{Pr_t}\frac{\varepsilon_m}{\nu}\right]\frac{\partial T^+}{\partial y^+}. \tag{6}$$

For a fully developed film undergoing evaporative heating, all the energy input at the wall is lost at the film interface making the left-hand side of equation (6) unity. Integrating this equation gives the temperature profile

$$T^+ = \int_0^{y^+} \frac{1}{\frac{1}{Pr} + \frac{1}{Pr_t}\frac{\varepsilon_m}{\nu}}\,dy^+. \tag{7}$$

Changing the upper integration limit of equation (7) to δ^+ gives the dimensionless wall temperature from which the dimensionless heat transfer coefficient can be determined

$$h_E^* = \frac{(\delta^+)^{1/3}\,Pr}{T_w^+}. \tag{8}$$

Equations (4)–(8) were solved numerically using

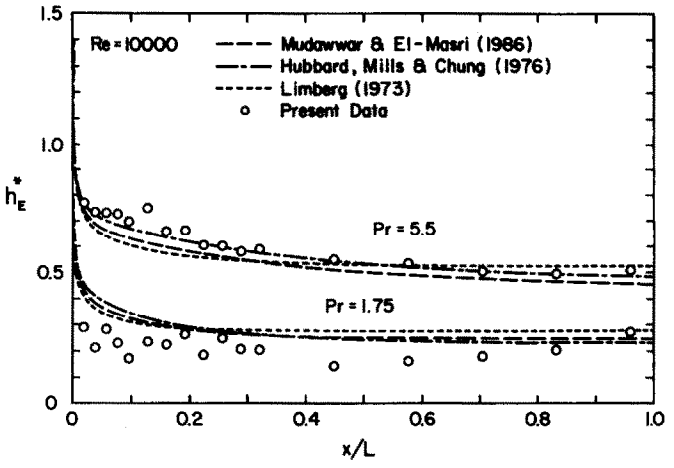

FIG. 12. Comparison of experimental data for evaporative heating with numerical predictions for the thermal development region.

Gauss–Legendre quadratures with sixth-degree Legendre polynomials.

In the second part of the numerical analysis, a finite difference scheme predicted heat transfer coefficients in the development region. The model assumed a fully developed velocity profile determined from the integration of equation (4). The discretized energy equations were solved over an equally spaced grid using a marching solution in the direction of fluid flow along the heated length, and the Thomas algorithm was used to solve the set of equations at each longitudinal position. Fully developed conditions were obtained from the asymptotic value of h_E and confirmed by direct integration of equation (7).

Figure 12 shows the development region predictions for evaporating films at a Reynolds number of 10 000. For a Prandtl number of 5.5, the models predicted the thermal development region fairly well, although Limberg's model reached an asymptotic value for h_E^* much earlier than the other two models. Fully developed conditions for these models were not reached until x/L was approximately 2.8, where L is the length of the experimental test section (781 mm).

The shorter development length for the lower Prandtl number was not predicted as well, although the scatter in the data makes an exact comparison difficult. For this case, Limberg's model predicted steady-state conditions for $x/L = 0.442$ while the models of Mudawwar and El-Masri and Hubbard *et al.* predicted fully developed conditions at $x/L \simeq 1.3$. None of the models predicted the gradual increase in h_E^* near the lower end of the heated length since they do not account for interfacial wave development in the direction of fluid flow.

For a Prandtl number of 5.5 the Limberg model compared well with the models of Hubbard *et al.* and Mudawwar and El-Masri in predicting h_E at $x = L$ with the former overpredicting the data and the later two models underpredicting the data. At lower Prandtl number, all of the models overpredicted the data. The failure to predict the data can be attributed to poor representation of wave induced turbulent activity at the film surface. As shown by equation (6), the conservation of the heat flux across the film results in the eddy diffusivity function seriously affecting the temperature distribution at the wall and at the film surface. This is in contrast to the case of sensible heating, where the left-hand side of equation (6) is zero at the film interface, making the heat transfer predictions less sensitive to the behavior of the eddy diffusivity function at the interface.

To substantiate the argument for the difference in development lengths for sensible heating and evaporation, predictions for the development of the temperature profile were found using the finite difference model, encompassing Mudawwar and El-Masri's eddy diffusivity model and a turbulent Prandtl number of 0.9.

Figures 13 and 14 show the temperature profiles for a Reynolds number of 10 000 and a Prandtl number of 5.5 for sensible heating and evaporation, respectively. The y-axis is represented as the ratio of position in

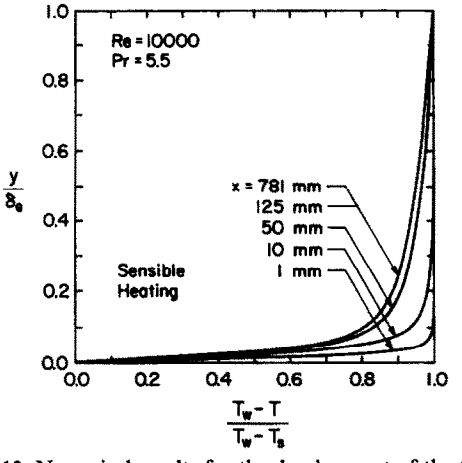

FIG. 13. Numerical results for the development of the temperature profile with heated length for sensible heating based on Mudawwar and El-Masri's model [15].

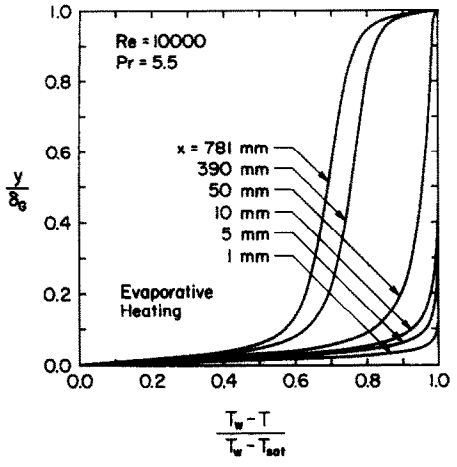

FIG. 14. Numerical results for the development of the temperature profile with heated length for evaporative heating based on Mudawwar and El-Masri's model [15].

the film to the film thickness calculated from the expression presented by Gimbutis [10]. The x-axis is the dimensionless temperature with the heating results referenced to the interface temperature, and the evaporation results referenced to the saturation temperature. The dimensionless temperatures are comparable since the assumed surface temperature of a film undergoing evaporation is T_{sat}.

As expected, the adiabatic condition at the film interface prevented the development of an interfacial temperature gradient for the case of sensible heating. The influence of the wall heat flux became noticeable at the film interface at approximately 50 mm, with fully developed conditions occurring at approximately 125 mm down the heated length. The temperature profile remained fairly constant from this position to the end of the heated length, $x = 781$ mm.

The initial development for the evaporation temperature profile was identical to that for sensible heating up to approximately 50 mm. At this point the effects of energy loss at the film interface can be observed by the development of an interfacial temperature gradient which led to changes in the thermal boundary layer over the entire length of the heated section. Thus, it appears that the increased development length necessary for saturated conditions is a result of the growth of a thermal resistance at the film interface.

5. CONCLUSIONS

The experimental results for evaporative heating of free-falling films have been presented. A gradual thermal boundary layer development, which persisted over more than one half the heated length, characterized the flow. An interfacial thermal resistance forming at the film interface—the result of evaporative energy transport—accounted for a large fraction of the length of the thermal development region. The interfacial temperature gradient appeared in measurements of the temperature profile and in numerical simulations. The heat transfer coefficients, averaged over the section of the heated length where the minimum values were seen to occur, correlated well as a function of Reynolds and Prandtl numbers.

Using existing eddy diffusivity models, numerical studies were performed to determine heat transfer coefficients in the development region and under fully developed conditions. The models predicted the behavior of the data in the early stages of development, but failed to accurately predict the heat transfer coefficients in the development region at lower Prandtl numbers. This discrepancy is evidence that turbulent activity at the film interface need to be better accounted for in a new film model which involves analysis of waves at the film interface. Development of such a model requires simultaneous measurements of the instantaneous film thickness and temperature distribution across the film at several locations in the direction of fluid flow, an effort presently undertaken at Purdue's Boiling and Two-phase Flow Laboratory as an extension of the present study.

Acknowledgement—The authors gratefully acknowledge the support of the U.S. Department of Energy, Office of Basic Sciences through Grant No. DE-FG02-85ER13398.

REFERENCES

1. H. Struve, Der warmeubergang an einen verdampfenden rieselfilm, *VDI ForschHft.* 534 (1969).
2. K. R. Chun and R. A. Seban, Heat transfer to evaporating liquid films, *J. Heat Transfer* **93,** 391–396 (1971).
3. T. Fujita and T. Ueda, Heat transfer to falling liquid films and film breakdown—II, *Int. J. Heat Mass Transfer* **21,** 109–118 (1978).
4. W. M. Rohsenow, J. H. Webber and A. T. Ling, Effect of vapour velocity on laminar and turbulent film condensation, *Trans. ASME* **78,** 1637–1643 (1956).
5. A. E. Dukler, Fluid mechanics and heat transfer in vertical falling-film systems, *Chem. Engng Prog.* **56,** 1–10 (1960).
6. A. Iribarne, A. D. Gosman and D. B. Spalding, A theoretical and experimental investigation of diffusion-controlled electrolytic mass transfer between a falling film and a wall, *Int. J. Heat Mass Transfer* **10,** 1661–1676 (1967).
7. H. R. Kunz and S. Yerazunis, An analysis of film condensation, film evaporation and single-phase heat transfer, ASME Paper No. 67-HT-1 (1967).
8. A. F. Mills and D. K. Chung, Heat transfer across turbulent falling films, *Int. J. Heat Mass Transfer* **16,** 694–696 (1973).
9. H. Limberg, Warmeubergang an turbulente und laminare rieselfilme, *Int. J. Heat Mass Transfer* **16,** 1691–1702 (1973).
10. G. Gimbutis, Heat transfer of a turbulent falling film, *Proc. 5th Int. Heat Transfer Conf.*, Tokyo, Japan, Vol. 2, pp. 85–89 (1974).
11. G. L. Hubbard, A. F. Mills and D. K. Chung, Heat transfer across a turbulent falling film with concurrent vapor flow, *J. Heat Transfer* **98,** 319–320 (1976).
12. R. A. Seban and A. Faghri, Evaporation and heating with turbulent falling liquid films, *J. Heat Transfer* **98,** 315–318 (1976).
13. O. C. Sandall, O. T. Hanna and C. L. Wilson, Heat

transfer across turbulent falling liquid films, *AIChE Symposium Series, Heat Transfer*, Niagara Falls, pp. 3–8 (1984).
14. V. P. Carey, A note on heat transfer to turbulent liquid falling films at high Prandtl number, *A.I.Ch.E. Jl* **31**, 1575–1577 (1985).
15. I. Mudawwar and M. A. El-Masri, Momentum and heat transfer across freely-falling turbulent liquid films, *Int. J. Multiphase Flow* **12**, 771–790 (1986).
16. A. P. Lamourelle and O. C. Sandall, Gas absorption into a turbulent liquid, *Chem. Engng Sci.* **27**, 1035–1043 (1972).
17. K. R. Chun, Evaporation from thin liquid films, Ph.D. Thesis, University of California, Berkeley (1969).
18. H. Ueda, R. Moller, S. Komori and T. Mizushima, Eddy diffusivity near the free surface of open channel flow, *Int. J. Heat Mass Transfer* **20**, 1127–1136 (1977).
19. J. A. Shmerler and I. A. Mudawwar, Local heat transfer coefficient in wavy free-falling turbulent liquid films undergoing uniform sensible heating, *Int. J. Heat Mass Transfer* **31**, 67–77 (1988).
20. J. G. Collier, *Convective Boiling and Condensation*, 2nd Edn, p. 152. McGraw-Hill, U.K. (1981).
21. J. A. Shmerler, A study of sensible heating and evaporation in free-falling liquid films, MSME thesis, Purdue University, West Lafayette, Indiana (1986).
22. J. G. Collier, *Convective Boiling and Condensation*, 2nd Edn, pp. 316–323. McGraw-Hill, U.K. (1981).
23. J. E. Koskie, I. Mudawwar and W. G. Tiederman, Characteristics of interfacial waves on free-falling liquid films, 4th Miami Int. Symposium on Multi-phase Transport and Particulate Phenomena, Miami, Florida, 15–17 December (1986).
24. H. Takahama and S. Kato, Longitudinal flow characteristics of vertically falling liquid films without concurrent gas flow, *Int. J. Multiphase Flow* **6**, 203–215 (1980).
25. L. K. Brumfield and T. G. Theofanous, On the prediction of heat transfer across turbulent liquid films, *J. Heat Transfer* **98**, 496–502 (1976).
26. A. S. Telles, Liquid film characteristics in vertical two-phase flow, Ph.D. thesis, University of Houston, Texas (1986).
27. K. J. Chu and A. E. Dukler, Statistical characteristics of thin, wavy films: Part II. Studies of the substrate and its wave structure, *A.I.Ch.E. Jl* **20**, 695–706 (1974).

COEFFICIENT LOCAL DE TRANSFERT DE CHALEUR EVAPORATOIRE DANS DES FILMS LIQUIDES TOMBANTS TURBULENTS

Résumé—On étudie expérimentalement et numériquement le chauffage évaporatif d'un film liquide turbulent en chute libre. Le film montre une grande longueur d'établissement thermique qui va jusqu'à plus de la moitié des 781 mm de longueur chauffée. La longueur accrue de la région d'etablissement est attribuée à la formation d'une couche limite à l'interface du film. Cette couche limite est prédite numériquement et observée par des mesures de température dans le film. Les coefficients de transfert thermique sont moyennés sur la section inférieure du tube et exprimés en fonction des nombres de Reynolds et de Prandtl. Des calculs numériques sont faits pour la région d'établissement et pour la région pleinement établie en utilisant trois modèles différents de viscosité turbulente. Une comparaison avec les données expérimentales révèle que deux de ces modèles sont très satisfaisants dans la prévision de l'étendue de la région d'établissement et du coefficient de transfert thermique évaporatif moyen dans le temps; néanmoins les données montrent le besoin d'un nouveau modèle qui prendrait en compte avec précision les variations locales et spaciales de l'épaisseur du film induites par les ondulations.

LOKALER WÄRMEÜBERGANGSKOEFFIZIENT BEI DER VERDAMPFUNG AN TURBULENTEN, FREI FALLENDEN FLÜSSIGKEITSFILMEN

Zusammenfassung—Die Verdampfung an einem frei fallenden turbulenten Flüssigkeitsfilm ist experimentell und numerisch untersucht worden. Der Film wies eine große thermische Einlauflänge auf; sie erstreckte sich über mehr als die Hälfte der 781 mm langen Heizstrecke. Die erhöhte Einlauflänge wird auf die Ausbildung einer Grenzschicht an der Filmoberfläche zurückgeführt. Diese Grenzschicht wurde numerisch vorhergesagt und bei Temperaturmessungen im Film beobachtet. Die Wärmeübergangskoeffizienten wurden im unteren Teil des Rohres gemittelt und als Funktion von Reynolds- und Prandtl-Zahl korreliert. Numerische Berechnungen der Wärmeübergangskoeffizienten wurden für die Einlaufstrecke und für den Bereich der voll ausgebildeten Strömung unter Verwendung dreier verschiedener Modelle für den turbulenten Transport durchgeführt. Der Vergleich mit den experimentellen Daten enthüllt, daß zwei dieser Modelle zum Berechnen der Ausdehnung des thermischen Einlaufs und des zeitlich gemitteften Wärmeübergangskoeffizienten bei der Verdampfung bedingt geeignet sind. Die Daten weisen auf die Notwendigkeit hin, ein neues Modell zu entwickeln, das lokale und räumliche welleninduzierte Variationen der Filmdicke genauer berücksichtigt.

ОПРЕДЕЛЕНИЕ ЛОКАЛЬНОГО КОЭФФИЦИЕНТА ТЕПЛООБМЕНА ПРИ ИСПАРЕНИИ СВОБОДНО СТЕКАЮЩИХ ТУРБУЛЕНТНЫХ ПЛЕНОК ЖИДКОСТИ

Аннотация—Экспериментально и численно исследовано испарение свободно стекающей турбулентной пленки жидкости. Пленка имела протяженный участок тепловой стабилизации, занимающий более половины длины нагревательного участка в 781 мм, что обусловлено образованием теплового пограничного слоя. Существование пограничного слоя было предсказано численно и подтверждено измерениями температуры в толще пленки. Коэффициенты теплопереноса усреднены по нижнему участку трубы и обобщены в виде функции чисел Рейнольдса и Прандтля. На основе трех различных моделей вихревой диффузии получены численные значения коэффициентов теплообмена для неустановившейся и полностью развитой областей. Сравнение с экспериментальными данными показывает, что с помощью двух из указанных моделей можно довольно точно рассчитать протяженность неустановившейся области, а также усредненный по времени коэффициент теплообмена, однако полученные результаты показывают, что необходима новая модель, которая бы точно учитывала локальные и пространственные изменения толщины пленки, вызываемые волновыми возмущениями.